FISEVIER

Contents lists available at ScienceDirect

Applied Surface Science Advances

journal homepage: www.sciencedirect.com/journal/applied-surface-science-advances





Air leakage in seals with application to syringes

N. Rodriguez *,a, A. Tiwari b,c, B.N.J. Persson b,c

- ^a BD Medical-Pharmaceutical Systems, 1 Becton Drive, Franklin Lakes NJ 07417, USA
- ^b Peter Grünberg Institute (PGI-1), Forschungszentrum Jülich, 52425 Jülich, Germany
- ^c Multiscale Consulting, Wolfshovener str. 2, Jülich 52428, Germany

ARTICLE INFO

Keywords:
Teflon coating
Syringe leakage
Ballistic gas flow
Contact mechanics
Elastoplasticity
Viscoelasticity
Plunger stopper
Glass syringe

ABSTRACT

We study the leakage of air in syringes with Teflon coated rubber stopper and glass barrel. The leakrate depends on the interfacial surface roughness, the viscoelastic properties of the rubber and on the elastoplastic properties of the Teflon coating. The measured leakage rates are compared to the predictions of a simple theory for gas flow, which takes into account both the diffusive and ballistic air flow, and the elastoplastic multiscale contact mechanics which determines the probability distribution of interfacial separations. The theory shows that the interfacial air flow (leakage) channels are so narrow that the gas flow is mainly ballistic (the so called Knudsen limit). The implications for container closure integrity is discussed.

1. Introduction

All solids have surface roughness, which has a huge influence on a large number of physical phenomena such as adhesion, friction, contact mechanics and the leakage of seals[1–14]. Thus when two solids with nominally flat surfaces are squeezed into contact, unless the applied squeezing pressure is high enough, or the elastic modulus of at least one of the solids low enough, a non-contact region will occur at the interface. If the non-contact region percolate, open flow channels exist, extending from one side of the nominal contact region to the other side. This will allow fluid to flow at the interface from a high fluid pressure region to a low pressure region.

We consider the leakage of air at the interface between a Teflon coated rubber stopper and a glass barrel. We have studied this problem in Ref[15]. but here we extend that study by using a new design of the stopper involving much higher contact pressures, where the contact is close to the percolation threshold.

Teflon (polytetrafluorethylen) and other films (e.g., ultra-high-molecular-weight polyethylene or ethylene-tetrafluorethylene-copolymer) are used in laminating rubber stoppers and have elastic modulus 100-1000 times higher than the typical rubbers stoppers (2-6 MPa). Thus, the average interfacial separation, resulting from the surface roughness, is much larger than for the uncoated rubber stopper, and the contact area percolation threshold may not be achieved. Therefore, in any laminated rubber stoppers an accurate calculation of

the interfacial separations as well as design parameters (contact pressure, geometry, etc...) is particularly important to assure container closure integrity, low weight losses, functional performance, and no microbial ingress during the shelf life and use of the product. One way to study the size of the most narrow constrictions in the open (percolating) channels at the stopper-barrel interface is by measuring the air leakage rate in syringes (with closed needle).

2. Experimental results

The Teflon laminated rubber stopper used in this study has three ribs $1{\text -}3$ which contact the glass barrel. The ribs have (half) circular cross-section with the front and middle ribs with the diameter 0.4 mm, and back rib 3 with the diameter 0.8 mm. We first determine the width and the average contact pressure acting in the contact region. We also study the surface topography of the Teflon surface on the ribs. Finally we present the results of the air leakage experiments.

2.1. Nominal contact width w

Using a Peak optical microscope (Model 2004) we have measured the contact width between the Teflon laminated rubber stopper and the glass barrel in the axial direction of the contact regions using a lens magnified with $10\times$ magnification and having a calibrated reticle of resolution of 0.1mm (see Fig. 1). The two inner ribs, 1 and 2, are

E-mail address: nestor.rodriguez@bd.com (N. Rodriguez).

https://doi.org/10.1016/j.apsadv.2022.100222

^{*} Corresponding author.

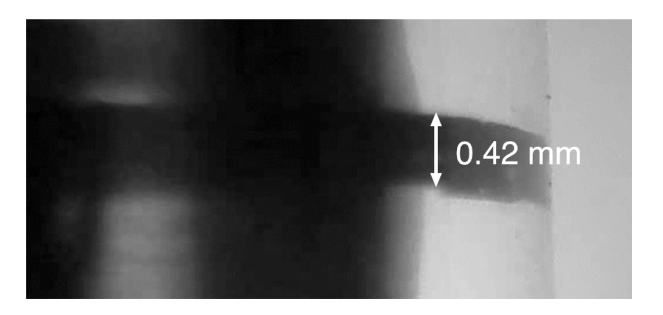


Fig. 1. Optical picture of the first rib contact region for Teflon laminated rubber stopper in a glass barrel. The front and the middle ribs, 1 and 2, are nominally identical and with contact width $w \approx 0.42$ mm in the axial direction. The third outer rib 3 is wider but the contact pressure much lower, and this rib has only a negligible influence on the air leakage rate.

nominally identical and with the contact width $w\approx 0.42$ mm. The third (outer) rib 3 is wider but the contact pressure is much lower, and this rib has only a small influence on the air leakage rate. Note that the pressure is so high as to fully flatten the rib 1 and 2. We will assume below that the contact pressure is Hertzian-like but this is only a rough estimation because of the large deformations involved.

The old design of the stopper studied in Ref[15]. had two ribs, the inner rib with rectangular cross section with the contact width \approx 1.2 mm and back rib circular with the diameter 1 mm. In this case the average contact pressure (\sim 1 MPa) is much lower than for the new design.

2.2. Average contact pressure p₀

We have measured the average contact pressure between the stopper and the barrel using the set-up shown in Fig. 2. Two steel blocks with a cylinder cavity with the same radius as the inner radius R of the barrel is squeezed together with the stopper in-between, with such a force F that the gap just closes without any repulsive force at the steel-steel contact.

We have used two different methods. In one method we connect electric wires to the two steel blocks and when electric contact occur a sound is produced in a loudspeaker and at that point we stop the compression movement and determine the compression force. In the second method we first determine the displacement which result in metal-metal contact when there is no rubber stopper in between. This position is determined by observing the rise in the force (the compression force vanish before contact) and can be easily determined accurately. After we separate the surfaces and insert the rubber stopper and

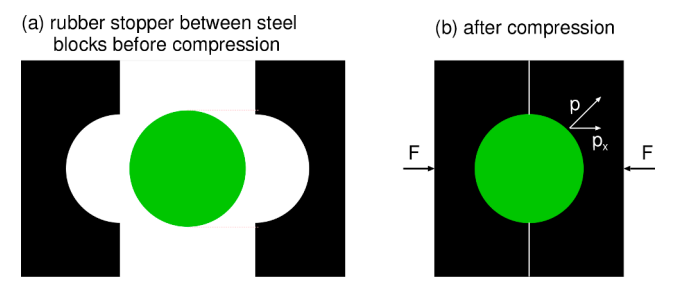


Fig. 2. Experimental method used to determine the radial force squeezing the stopper against the barrel. Two steel blocks with a cylinder cavity with the same radius as the inner radius R of the barrel is squeezed together, with the rubber stopper inserted, with such a force F that the gap just closes without any repulsive force from the steel-steel contact. The steel surfaces are lubricated so negligible shear stress occur in the contact between the stopper and the steel surface. The average pressure p_0 acting in the contact region between the stopper and the steel surface is determined by $p_0Dw = F$, where w is the width in the axial direction of the contact region and D = 2R the inner diameter of the barrel.

move the upper block towards the lower block to the pre-determined position. We note that a very stiff mechanical set-up is needed for this study.

After compressing the rubber stopper as described above we study the compression force as a function of time (since the compression force decreases with increasing time due to viscoelastic relaxation). The contact pressure initially drop rather rapidly in time but after some time much slower and we use the contact force obtained after ~ 1 hour of contact time. Fig. 3 illustrate the viscoelastic relaxation but for stopper not used in the present study. The red and green line are repeating the experiment for two nominally identical stoppers. The vertical dashed lines indicate the time 1 h and 1 year.

In the present study we used an Instron tensile test bench (model 5542) equipped with a load cell of 100N with a resolution of \approx 0.2N to squeeze the blocks. The steel surfaces are lubricated so negligible shear stress occurs in the contact between the stopper and the steel surface. If w is the width in the axial direction of the contact region and if p_0 denotes the average pressure acting in the contact region between the stopper and the steel surface then

$$F = \int_{-\pi/2}^{\pi/2} d\phi \ wRp_0 \cos\phi = 2wRp_0.$$
 (1)

Thus $p_0=F/wD$ where D=2R is the inner diameter of the barrel. Using this equation we can determine the average pressure acting on each rib by removing the other ribs. In the present case this shows that for the inner two ribs 1 and 2 (which are nominal identical with contact width $w\approx 0.42$ mm), the (average) contact pressure $p_0\approx 3.2$ MPa, and the maximal (Hertz) contact pressure $p_{\rm max}=3p_0/2\approx 4.8$ MPa, where we have used D=6 mm. The third (outermost) rib 3 is wider but the contact pressure much smaller, so this rib does not affect the air leakage rate.

2.3. Surface roughness power spectrum

The most important information about the surface topography of a rough surface is the surface roughness power spectrum.

We have measured the surface roughness profile using a stylus instrument [Mitutoyo Portable Surface Roughness Measurement Surftest SJ-410 with a diamond tip with the radius of curvature $r_0=1~\mu m$, and with the tip-substrate repulsive force $F_{\rm N}=0.75~{\rm mN}$ and the tip speed $v=50~\mu m/{\rm s}$], and calculated the surface roughness power spectrum as described in detail elsewhere [6]. For a one-dimensional (1D) line scan

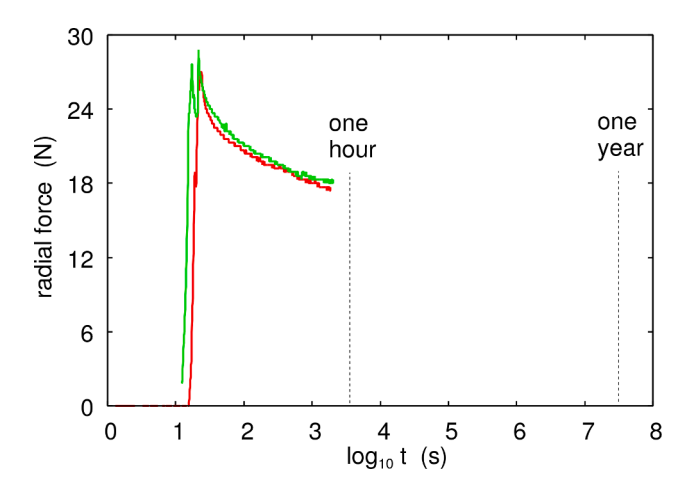


Fig. 3. The measured radial force for a stopper as a function of the logarithm of time. The red and green line are repeating the experiment for two nominally identical stoppers. The vertical dashed lines indicate the time 1 h and 1 year. (For interpretation of the references to colour in this figure legend, the reader is referred to the web version of this article.)

z = h(x) the power spectrum is given by

$$C_{1D}(q) = \frac{1}{2\pi} \int dx \ \langle h(x)h(0)\rangle e^{iqx} \qquad (2)$$

where $\langle . \rangle$ stands for ensemble averaging. For surfaces with isotropic roughness the 2D power spectrum C(q) can be obtained directly from $C_{\mathrm{1D}}(q)$ as described elsewhere [16,17]. For randomly rough surfaces, all the (ensemble averaged) information about the surface is contained in the power spectrum C(q) (see Ref[5,6].). For this reason the only information about the surface roughness which enter in contact mechanics theories (with or without adhesion) is the function C(q). Thus, the (ensemble averaged) area of real contact, the interfacial stress distribution, and the distribution of interfacial separations, are all determined by C(q).

Fig. 4 shows the surface height along a rib on the Teflon coated rubber stopper. We have removed the curvature from the rib. The height h(x) is given in μ m as a function of the distance x in mm.

The dashed lines in Fig. 5 shows the surface roughness power spectra obtained from stylus topography measurements on the rib 1 (red) and rib 2 (blue). The solid lines are the effective power spectra of the plastically deformed Teflon surfaces obtained as described in Ref[18]. and summarized below and in the Appendix. In the calculation we have used the rubber modulus E=4.6 MPa and Poisson ratio $\nu=0.5$, the Teflon film thickness $d=15~\mu\text{m}$, the Teflon modulus E=500~MPa and Poisson ratio $\nu = 0.4$, and the Teflon penetration hardness $\sigma_P = 13$ MPa. The penetration hardness of Teflon (without filler) is typically in the range 20 – 30 MPa, but we interpret the lower penetration hardness we use as an effective hardness as the Teflon surface is exposed also to shear stresses and wear processes as it moves in the glass barrel, which smooth the surface. In addition, some plastic flow occur already when the contact pressure is well below the penetration hardness[19]. In fact, it has been observed that Teflon start to flow plastically around 13 MPa in wear experiments[20].

Here we note that the Persson contact mechanics theory assumes randomly rough surface roughness. However, plastic deformation in general result in non-random roughness. The procedure we use to obtain the power spectrum for plastically deformed surfaces has been described in detail elsewhere [18] but is briefly summarized here.

In elastic contact mechanics the contact area decreases continuously as we increase the magnification and observe shorter wavelength roughness. Hence, when a solid with surface roughness is squeezed against a flat rigid surface with the force F_N the solid may deform elastically in the contact regions observed at low magnification, where the contact area A is large and the contact stress F_N/A low, but plastically above some critical magnification which depends on the penetra-

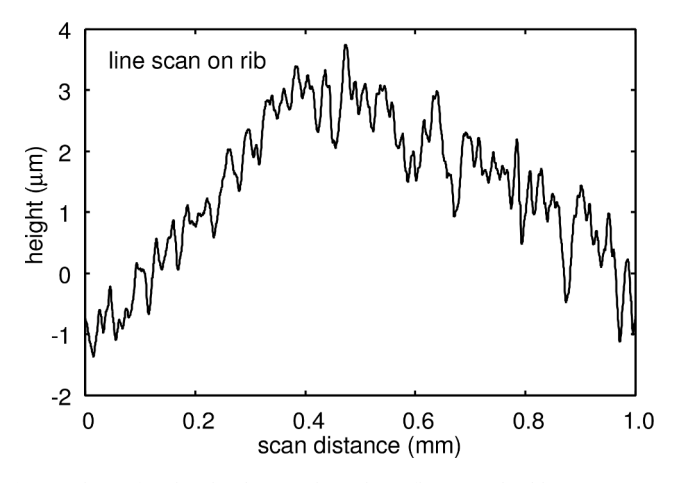


Fig. 4. The surface height along a rib on the Teflon coated rubber stopper. We have removed the curvature from the rib. The height h(x) is given in μm as a function of the distance x in mm.

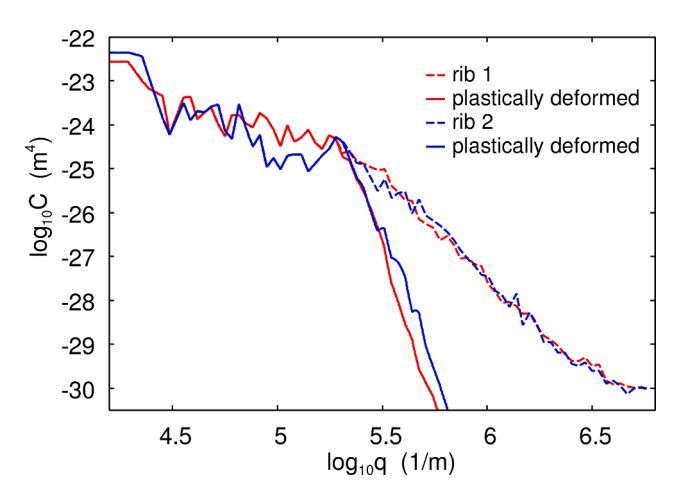


Fig. 5. The surface roughness power spectra obtained from stylus topography measurements on the inner rib 1 (red) and the next inner rib 2 (blue). The solid lines are the effective power spectra of the plastically deformed Teflon surfaces using the Teflon penetration hardness $\sigma_P=13$ MPa. (For interpretation of the references to colour in this figure legend, the reader is referred to the web version of this article.)

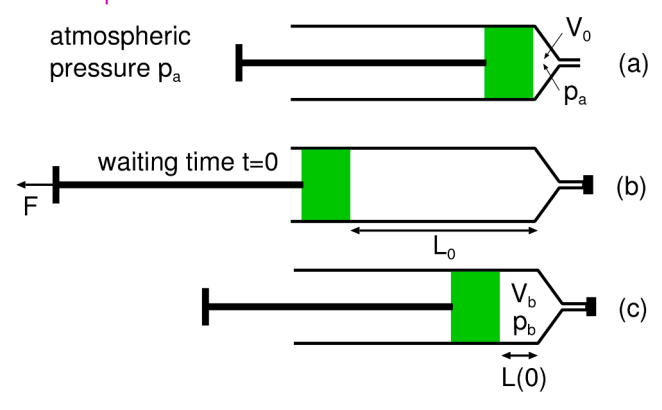
tion hardness. We take this plastic deformation into account by smoothing (or removing) the short wavelength roughness. We do this in such a way that the elastic contact area of the plastically deformed surface will be the same (as a function of magnification) as that obtained using the Persson elastoplastic contact mechanics theory[21,22]. But in order for the surface to be randomly rough one must smooth the surface everywhere, i.e., also in the non-contact area. We have argued before[5, 23] that this has only a small influence of the interfacial separation in the open flow channels relevant for the fluid leakage problem. Nevertheless, the power spectrum obtained this way is an effective power spectrum designed for special purpose, and it cannot be compared to the real power spectrum obtained from the surface topography of the plastically deformed surface, as discussed in our earlier studies[24].

2.4. Leakage rate

We have measured the air leakage in 15 syringes using the same procedure as in Ref[15]. and summarized in Fig. 6. We first assemble the barrel-stopper in empty configuration with the stopper pushed to the end of the barrel, resulting in a small volume V_0 of gas in the syringe at atmospheric pressure. Next the needle is closed so no air can penetrate into the syringe from the needle side, and the stopper is pulled back (retracted) to full fill position resulting in a volume L_0A_0 of gas at low pressure. In the first experiment the pull-force is immediately removed, which results in the stopper moving to a new position L(0) where the gas pressure p_b is such that the pressure force $(p_a - p_b)A_0$ (due to the difference in the gas pressure outside and inside the barrel) is equal to the stopper-barrel friction force. Next we repeat the experiment except now the stopper is kept in the pulled back (retracted) position for some time t_1 . This results (due to air leakage at the barrel-stopper interface) in an increase in the air pressure, and when the pull force is removed after some time t_1 the stopper will move to a new position with $L(t_1) > L(0)$. The volume increase $\Delta V = [L(t_1) - L(0)]A_0$ is due to the air leakage into the syringe. However, the air pressure in the volume ΔV is not the atmospheric air pressure p_a but is equal to p_b . Thus, the ΔV correspond to a volume $\Delta V_{\rm a} = \Delta V p_{\rm b}/p_{\rm a}$ of air of atmospheric pressure. Since no leakage is assumed to occur during the first experiment we have $p_aV_0=p_bV_b$ so that $p_b/p_a = V_0/V_b$. Hence the volume of air of atmospheric pressure leaking into the syringe per unit time equal

$$\dot{V} = \frac{\Delta V_{\rm a}}{t_1} = \frac{\Delta V}{t_1} \frac{p_{\rm b}}{p_{\rm a}} = \frac{\Delta V}{t_1} \frac{V_0}{V_{\rm b}}$$
 (3)

First experiment:



Second experiment:

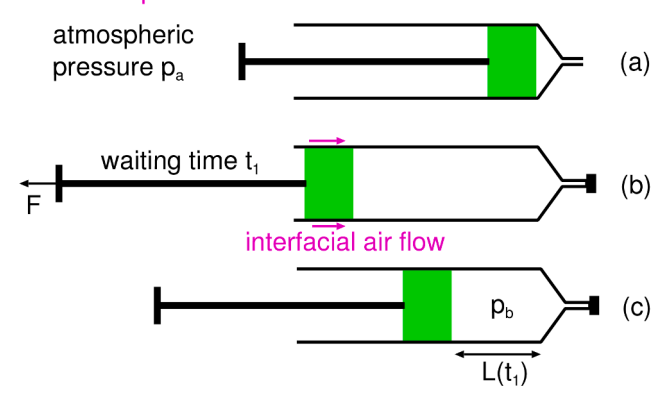


Fig. 6. Experiments performed in order to measure the air leak-rate of syringes (see text for details).

This method to study the air leakage is very accurate and we can measure arbitrary small leakage rates by waiting long time enough with the rubber stopper in the displaced state [see (b) in Fig. 6 (bottom part)]. Of course there may be a contribution to the leakage by air molecules diffusing through the rubber matrix. However we also performed leakage experiments with silicone oil lubricated glass barrels, where the air flow channels may be blocked by the oil. These experiments gave leakage rates typically 1 or 2 orders of magnitude smaller than for the non-lubricated barrels, which indicates an upper limit for the order of magnitude of air diffusion through the laminated rubber stopper.

It is easy to study the leakage for each rib separately by introducing a thin cut in the other ribs through which the air (or fluid) can move with negligible resistance. The final position of the stopper was measured with a rule (Starret model C330) and its resolution was ± 0.5 mm. So, the estimated error in the leakage data reported in Fig. 8 caused by the position uncertainty is less than $10^{-6}~\text{mm}^3/\text{s}.$

In our experiments, the pressure difference between inside and outside the syringe is about 1 bar, and the average air leakage rate about $2.2 \times 10^{-4} \text{ mm}^3/\text{s}$. We repeated the test in five of the fifteen syringes obtaining very similar leakage result as in the initial measurements. In an earlier study (see Ref[15].) with a different design of the Teflon coated rubber stopper, where the average contact pressure was much smaller, we observed larger air leakage rates, of order $4.8 \times 10^{-3} \text{ mm}^3/\text{s}$, i.e. about a factor of 20 higher than for the new design.

3. Analysis of leakage experiments

In syringe applications the separation between the surfaces at the most narrow constrictions (critical constrictions) along the biggest open flow channels are (almost) always smaller than the air gas molecule mean free path (which is about 60 nm for N_2 at 1 atm pressure). In fact,

for not-laminated rubber stoppers the contact area usually percolate and no gas or fluid leakage occurs. For teflon laminated rubber stoppers the contact area does not percolate but the separation between the surfaces in the critical constrictions (as predicted by the theory) is still so small (about 2 and 25 nm for the systems studied below) that collision between the air molecules in the critical constriction can be neglegted (ballistic motion), the so called Knudsen limit of gas flow.

The leakrate of fluids at interfaces between solids with random roughness can be calculated using the critical junction theory or the Bruggeman effective medium theory as described in detail elsewhere [27–35]. In the critical junction theory it is assumed that all the pressure drop in the fluid occurs at the most narrow constrictions along the biggest open (percolating) flow channels. The more accurate effective medium theory includes all flow channels in an approximate way but both theories gives usually very similar results. The probability distribution of interfacial separations, which enter in the theory for the leakage rate, is determined using the Persson contact mechanics theory [21,28,36–38]. In the present case, with the rubber stopper covered by a thin Teflon film, one must include the plastic deformations of the Teflon surface roughness profile, see Section 2 and Ref[18].

For the leakage of fluids one can usually assume laminar flow of Newtonian fluid characterized by a viscosity η . This description is also valid for gases if the surface separation at the critical constriction is much larger than the gas molecule mean free path λ . However, this is not the case in the present application where the flow through the critical constriction is ballistic rather than diffusive, see Fig. 7. Here ballistic refer only to the absence of collisions between the air molecules; the molecules may still scatter diffusely from the solid walls so the motion of gas molecules through the junction is always diffusive-like. In Ref[26, 39], we have presented an interpolation formula for gas flow through a narrow pore with the surface separation $u_{\rm c}$ much smaller than the width and length of the pore which correctly describes both the diffusive (large pore diameter) and ballistic (narrow pore diameter) limits:

$$\dot{N_{\rm b}} = \frac{1}{24} \frac{\left(p_{\rm a}^2 - p_{\rm b}^2\right)}{k_{\rm B}T} \frac{u_{\rm c}^3}{\eta} \left(1 + 12 \frac{\eta \overline{\nu}}{(p_{\rm a} + p_{\rm b})u_{\rm c}}\right) \tag{4}$$

In (4) enters the viscosity η and the average velocity \overline{v} of a gas molecules. The pressure inside and outside of the syringe are denoted by $p_{\rm b}$ and $p_{\rm a}$, respectively, and $k_{\rm B}T$ is the thermal energy ($k_{\rm B}$ is Boltzman constant and T the absolute temperature). Here we have assumed that the width and length L of the pore are equal and much larger than the separation $u_{\rm c}$ between the surfaces at the pore as predicted by theory (typically $u_{\rm c}/L\approx 0.01$). In the present study we have used $\eta=1.76\times 10^{-5}$ Pas

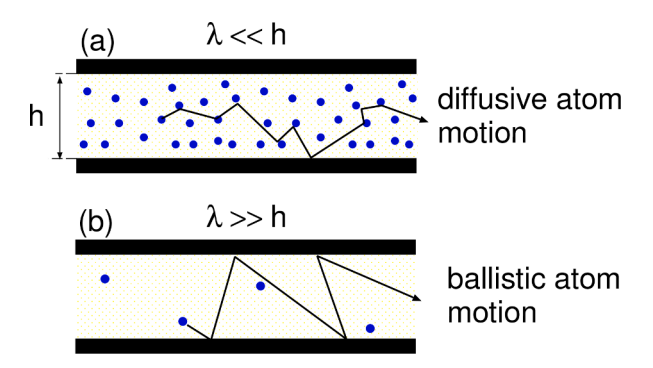


Fig. 7. Diffusive (a) and ballistic (b) motion of the gas atoms (e.g. He) in the critical junction. In case (a) the gas mean free path λ is much smaller than the gap width $h=u_{\rm c}$ and the gas molecules makes many collisions with other gas molecules before a collision with the solid walls. In the opposite limit, when $\lambda > u_{\rm c}$ the gas molecules makes many collisions with the solid wall before colliding with another gas molecule. In the first case (a) the gas can be treated as a (compressible) fluid, while a kinetic approach is needed in case (b). In the present applications $\lambda \approx 60$ nm (for N_2 at 1 atm pressure) while $u_{\rm c} \approx 2$ and ≈ 25 nm for the two systems studied below.

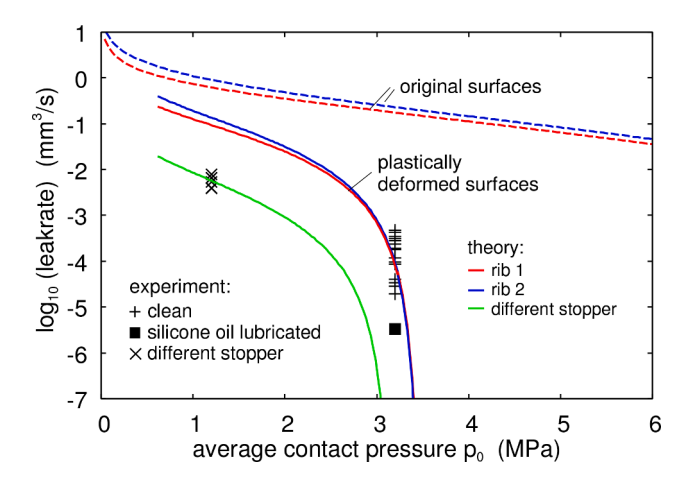


Fig. 8. Solid and dashed lines are the calculated leakage rate (obtained from theory) as a function of the average contact pressure using the plastically deformed surface (solid lines) and the original surface (dashed lines). The + symbols are the measured leakage rates using different (but nominally identical) clean syringes. The square symbol is for the same type of syringe but with the glass barrel lubricated by silicone oil. The \times symbols are for a different Teflon coated rubber stopper where the rib contact regions are much wider and the contact pressure much smaller (see Ref[15].).

(corresponding to a molecule mean-free path $\lambda = 59$ nm), and $\bar{\nu} = 470$ m/s. Other analytical and numerical treatments, which take in to account the effect of surface roughness, lengthscale and plasticity in the leakage prediction, are reported in the literature [9–13].

The solid and dashed lines in Fig. 8 shows the calculated leakage rate as a function of the average contact pressure using the plastically deformed surface (solid lines) and the original surface (dashed lines). The + symbols are the measured leakage rates using 15 different (but nominally identical) clean syringes. If the leakrate is measured in mm^3/s , then the average logarithmic leakrate is -3.01 with the standard deviation ± 0.46 . The square symbol is for the same type of syringe, but with the glass barrel lubricated by silicone oil. The silicone oil block air flow channels and reduces the air leakage rate, and in this case the air leakage may result from diffusion of air molecules through the stopper. Note the crucial influence of the plastic deformation which for the relevant average contact pressure $p_0\approx 3.2$ MPa reduces the leakage rate by a factor of ~ 1000 .

The maximum contact pressure for the rib contacts 1 and 2 is very close to the pressure where the contact area percolate. This result in the large fluctuations (by a factor of nearly 100) in the measured leakage rate between nominally identical syringes, and also in a large sensitivity in the calculated leakage rate to small variations in the system parameters, e.g., the penetration hardness.

The \times symbols in Fig. 8 are for a different Teflon coated rubber stopper studied in Ref[15]., where the rib contact regions are much wider and the contact pressure much smaller. For this stopper the Teflon coating was slightly smoother (see Fig. 9) than in this study, and when this is taken into account the theory prediction agrees very well with the measured data. This is shown by the green line in Fig. 8, which was calculated using the power spectrum of the plastically deformed surface obtained in the same way as for the rib 1 and 2. Note that the fluctuations in the measured data is much smaller than for the new stopper design, which is consistent with the fact that the contact pressure is well below the pressure where the contact area percolate.

The second term in the big parenthesis in (4) is the ratio between the leakage values through the critical constriction assuming purely ballistic and diffusive transport. This term can also be written as $\xi\langle\lambda\rangle/u_c$ where $\xi=32/\pi$ and where $\langle\lambda\rangle$ is an average mean free path due to collisions between the gas molecules in the junction[39]. Since $\xi\approx10$ it is clear that the ballistic transport will dominate when $u_c<10\langle\lambda\rangle$. Figure. 10

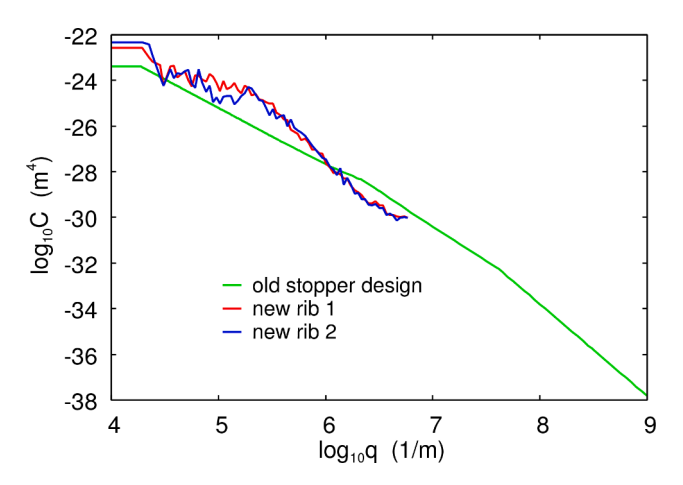


Fig. 9. The surface roughness power spectra obtained from stylus topography measurements on the inner rib 1 (red) and the next inner rib 2 (blue). The green line is the power spectrum for another design of the laminated rubber stopper with much wider rib contact regions. For this stopper both engineering stylus, optical and Atomic Force Microscopy topography was perform and the green line is a fit to all the measured data (see Ref[15].). (For interpretation of the references to colour in this figure legend, the reader is referred to the web version of this article.)

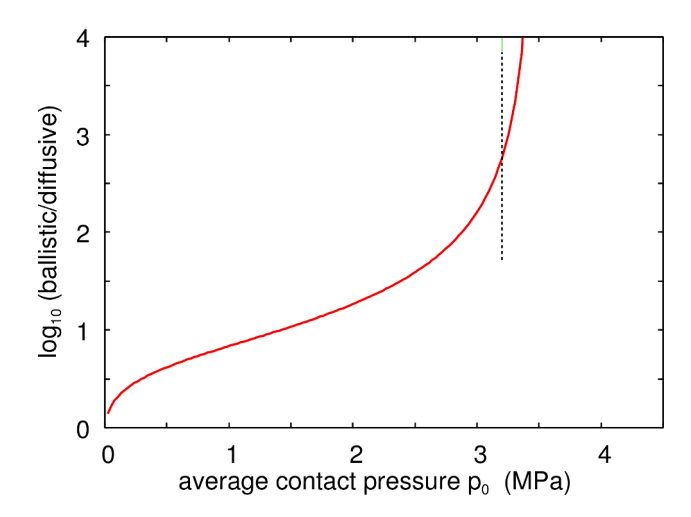


Fig. 10. The logarithm of the ratio between the leakage rate obtained assuming purely ballistic and diffusive transport as a function of the average contact pressure.

shows the ratio between the leakage rate obtained assuming purely ballistic and diffusive transport. For the case interesting us (dashed vertical line in the figure) the former gives ~ 560 times higher leakrate. This is because we are close to the percolation limit where the surface separation at the critical separation is very small.

For a randomly rough surface the contact area percolate when $A/A_0 \approx 0.42$ (see Ref[29].). When the contact area percolate no open flow channel occurs at the interface and the leakage rate vanish. Fig. 11 shows the contact area as a function of the contact pressure for rib 1. The solid line is for the plastically deformed surface and the dashed line for the originally (not deformed) Teflon surface. The dashed lines indicate the average and the maximum contact pressure assuming Hertz-like pressure distribution. Note that for the maximum contact pressure the contact area nearly percolate.

Container closure integrity is very important for syringes, so that no microorganism (bacteria and viruses) can penetrate from the outside to inside the syringe. The diameter of virus is in the range $\approx 20-400~\text{nm}$ and it is clear that complete container closure integrity would imply that

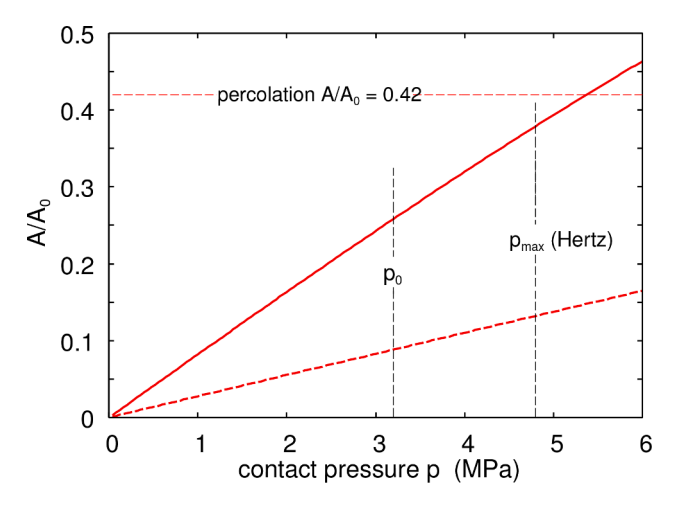


Fig. 11. The contact area as a function of the contact pressure for rib 1. The solid line is for the plastically deformed surface and the dashed line for the originally (not deformed) Teflon surface. The contact area for a randomly rough surface percolate when $A/A_0 \approx 0.42$. The dashed lines indicate the average and the maximum contact pressure assuming Hertz-like pressure distribution.

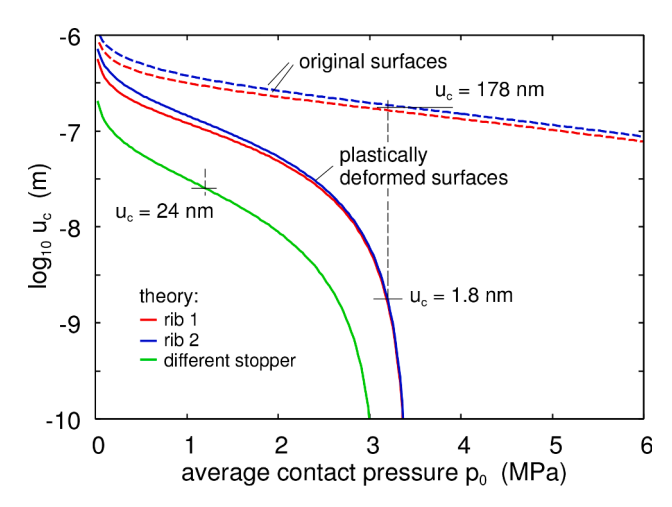


Fig. 12. The calculated surface separation at the critical constriction as a function of the average contact pressure using the plastically deformed surface (solid lines) and the original surface (dashed lines). The critical constriction is the most narrow constriction along the biggest open flow channels at the Teflon-glass interface.

the most narrow junction (denoted critical junction) in the largest open (non-contact) interfacial channel should be at most 20 nm. When this condition is satisfied, the fluid leakage is also negligible.

Fig. 12 shows the calculated surface separation at the critical constriction as a function of the average contact pressure using the plastically deformed surface (solid lines) and the original surface (dashed lines). The critical constriction is the most narrow constriction along the biggest open flow channels at the Teflon-glass interface. The separation of the surfaces at the critical constriction is $\sim 2\ \mathrm{nm}$, which implies that the container closure integrity and sterility is maintained.

The theory predict that the separation between the surfaces at the most narrow constrictions along the biggest fluid flow channels is so small (~ 24 nm) that also for the old design no bacterial ingress is possible, which has been confirmed experimentally.

4. Discussion

The study presented in this paper and in Ref[15,40]. shows the importance of plastic flow in some applications to seals. The good agreement found here, and in Ref[15]., support the procedure we use to include the plastic deformation. The role of plastic deformation was studied for metallic seals in Ref[40]. where the theory showed that the plastic flow reduce the leakage rate with a factor of \sim 8, resulting in water leakage rates in good agreement with experiments. We have shown in Ref[24,41]. that plastic flow may modify the surface topography in different ways for metals and polymers, but at least for Teflon and steel the way we include plastic flow gives good results for both systems.

We note that the interfacial separations predicted by the theory for the new and old stopper design (2 - 25 nm) are so small that gas leakage through molecular diffusion in the elastomer material[25,26] may contribute in an important way to the measured leakage rate. In fact, for the syringe lubricated by silicone oil, where $\dot{V}\approx 2.5\times 10^{-6}~\text{mm}^3/\text{s}$, this might be the dominant leakage mechanism. As a consequence the traditional way of container closure integrity studies (dye ingress or gas transport through the interface) is a subject of debate nowadays.

The present study assumes that there is no frictional shear stress at the interface between the Teflon film and the glass barrel. It has recently been shown that a shear stresses may influence the contact mechanics and the distribution of interfacial separations and hence the leakage rate [42,43]. Teflon against glass has a relative small friction coefficient but we cannot exclude that there may be some influence of the shear stress on the leakage rate. We also note that a shear stress may affect the area of real contact since the penetration hardness may be affected by the shear stress[20].

5. Summary and conclusion

We have performed air leakage experiments for the contact between a rubber stopper, laminated with a thin Teflon film, and a smooth cylindrical glass barrel. The measured leakrates were compared with theory predictions based on a theory involving gas flow through narrow constrictions taking into account the interfacial separation and meanfree path of the gas molecules. We used the Persson's contact mechanics theory to calculate the probability distribution of surface separation at the stopper/glass interface, and the Bruggeman effective medium theory to calculate the fluid flow resistance in the complex set of interconnected flow channels at the interface. We found that the plastic deformation of the Teflon surface reduces the interfacial separation by a factor of ~ 100 , and result in a reduction of the leakrate by a factor of ~ 1000 . The measured leakage rates are in good agreement with the theory predictions, but exhibit large fluctuations because the contact is close to the percolation threshold where small variations in the system parameters can generate large changes in the leakage rate.

Declaration of competing interest

The authors declare that they have no known competing financial interests or personal relationships that could have appeared to influence the work reported in this paper.

Acknowledgments

We thank Martin Müser for useful comments on the manuscript. We thank Lucile Gontard for checking some roughness parameters.

Appendix A. Accounting for plastic deformations

In the present study we are interested in Teflon coated rubber and in this case plastic deformation of the Teflon film is very important. Plastic flow is a complex topic but two very simple approaches have been proposed to take into account plastic deformations in practical situations. One approach, which is simple to implement when using actual realizations of the rough surfaces (as done in most numerically treatments, e.g., using the boundary element method [44]), is to move surface grid points vertically in such a way that the stress in the plastically deformed region is equal to (or below) the penetration hardness.

Another approach, which is more convenient in analytic contact mechanics theories, is based on smoothing the surface in wavevector space (see [27,28,45]). Thus, if two solids are squeezed together with the pressure p_0 they will deform elastically and, at short enough length scale, plastically. If the contact is now removed the surfaces will be locally plastically deformed. Assume now that the surfaces are moved into contact again at exactly the same position as the original contact, and with the same squeezing pressure p_0 applied. In this case the solids will deform purely elastically and the Persson contact mechanics theory can be (approximately) applied assuming that the surface roughness power spectrum $C_{\rm pl}(q)$ of the (plastically) deformed surface is known.

An expression for $C_{\rm pl}(q)$ can be obtained as follows. Let us consider the contact between two elastoplastic bodies with nominal flat surfaces, but with surface roughness extending over many decades in length scale, as is almost always the case. Assume that the applied (nominal) contact pressure p_0 is smaller than the penetration hardness σ_P of the solids. When we study the contact between the solids at low magnification we do not observe any surface roughness, and since $p_0 < \sigma_P$ the solids deform purely elastically at this length scale. As we increase the magnification we observe surface roughness and the (elastic) contact area decreases. At some magnification the pressure $p = p_0 A_0 / A(\zeta)$ may reach the penetration hardness and at this point all the contact regions are plastically deformed. In general, depending on the magnification ζ , some fraction of the contact area involves elastic deformations, while the other fraction has undergone plastic deformation. Thus we can write the contact area $A(\zeta) = A_{\rm el}(\zeta) + A_{\rm pl}(\zeta)$. The Persson contact mechanics theory predicts both $A_{\rm el}(\zeta)$ and $A_{\rm pl}(\zeta)$ (see Ref[21].).

In ref[18], we have shown that $C_{\rm pl}(q)$ can be obtained approximately using (with $\zeta=q/q_0$, where q_0 is the smallest wavenumber)

$$C_{\rm pl}(q) = \left[1 - \left(\frac{A_{\rm pl}(\zeta)}{A_{\rm pl}^0}\right)^6\right] C(q), \qquad (A1)$$

where $A_{\rm pl}^0 = F_{\rm N}/\sigma_{\rm P}$ is the contact area assuming that all contact regions have yielded plastically so the pressure in all contact regions equal the penetration hardness $\sigma_{\rm P}$. The basic picture behind this definition is that surface roughness at short length scales gets smoothed out by plastic deformation, resulting in an effective cut-off of the power spectrum for large wave vectors (corresponding to short distances). Assuming elastic contact and using the power spectrum (A1) result in virtually the same (numerical) contact area $A(\zeta)$, as a function of magnification ζ , as predicted for the original surface using the elastoplastic contact mechanics theory, where $A(\zeta) = A_{\rm el}(\zeta) + A_{\rm pl}(\zeta)$.

The smoothing of the surface profile at short length scale allow the surfaces to approach each other and will reduce the height u_c of the critical constriction. By using the plastically deformed surface roughness power spectrum (A1) this effect is taken into account in a simple approximate way.

It is not clear which of the two ways to include plastic flow described above is most accurate. In the first approach the solids deform plastically only in the region where they make contact, but this procedure does not conserve the volume of the solids. The second approach does conserve the volume but smooth the surfaces everywhere, i.e., even in the non-contact region. However, this does not influence the area of real contact, and it has a relative small influence on the surface separations in the big fluid flow channels, which mainly determine the fluid leakage rate (see Ref[24,41]. for a discussion of this).

References

- B.N.J. Persson, Sliding friction: Physical principles and applications, Springer, Heidelberg, 2000.
- [2] E. Gnecco, E. Meyer, Elements of friction theory and nanotribology, Cambridge University Press, 2015.
- [3] J.N. Israelachvili, Intermolecular and surface forces, (academic, london), 3rd ed, 2011.
- [4] J.R. Barber, Contact mechanics (solid mechanics and its applications), Springer, 2018.
- [5] B.N.J. Persson, Contact mechanics for randomly rough surfaces, Surf. Sci. Rep. 61 (201) (2006).
- [6] B.N.J. Persson, O. Albohr, U. Tartaglino, A.I. Volokitin, E. Tosatti, On the nature of surface roughness with application to contact mechanics, sealing, rubber friction and adhesion, J. Phys.: Condens. Matter 17 (2005).R1
- [7] M.H. Müser, W.B. Dapp, R. Bugnicourt, P. Sainsot, N. Lesaffre, T.A. Lubrecht, B.N. J. Persson, K. Harris, A. Bennett, K. Schulze, S. Rohde, P. Ifju, W.G. Sawyer, T. Angelini, H.A. Esfahani, M. Kadkhodaei, S. Akbarzadeh, J.-J. Wu, G. Vorlaufer, A. Vernes, S. Solhjoo, A.I. Vakis, R.L. Jackson, Y. Xu, J. Streator, A. Rostami, D. Dini, S. Medina, G. Carbone, F. Bottiglione, L. Afferrante, J. Monti, L. Pastewka, M.O. Robbins, J.A. Greenwood, Meeting the contact-mechanics challenge, Tribol. Lett. 65 (118) (2017).
- [8] A.I. Vakis, V.A. Yastrebov, J. Scheibert, C. Minfray, L. Nicola, D. Dini, A. Almqvist, M. Paggi, S. Lee, G. Limbert, J.F. Molinari, G. Anciaux, R. Aghababaei, S. E. Restrepo, A. Papangelo, A. Cammarata, P. Nicolini, C. Putignano, G. Carbone, M. Ciavarella, S. Stupkiewicz, J. Lengiewicz, G. Costagliola, F. Bosia, R. Guarino, N. M. Pugno, M.H. Müser, Modeling and simulation in tribology across scales: an overview, Tribol. Int. 125 (169) (2018).
- [9] A.A. Polycarpou, I. Etsion, Static sealing performance of gas mechanical seals including surface roughness and rarefaction effects, Tribol. Trans. 41 (531) (1988).

- [10] A.A. Polycarpou, I. Etsion, A model for the static sealing performance of compliant metallic gas seals including surface roughness and rarefaction effects, Tribol. Trans. 43 (237) (2000).
- [11] F. Bottiglione, G. Carbone, G. Mantriota, Fluid leakage in seals: an approach based on percolation theory, Tribol. Int. 42 (731) (2009).
- [12] F. Bottiglione, G. Carbone, L. Mangialardi, G. Mantriota, Leakage mechanism in flat seals, J. Appl. Phys. 106 (2009) 104902.
- [13] F. Perez-Rafols, R. Larsson, A. Almqvist, Modelling of leakage on metal-to-metal seals, Tribol. Int. 94 (421) (2016).
- [14] A. Tiwari, S.N. Shubin, B. Alcock, A.B. Freidin, B. Thorkildsen, A.T. Echtermeyer, Feasibility of using microencapsulated phase change materials as filler for improving low temperature performance of rubber sealing materials, Soft Matter. 13 (7760) (2017).
- [15] B. Lorenz, N. Rodriguez, P. Mangiagalli, B.N.J. Persson, Role of hydrophobicity on interfacial fluid flow: theory and some applications, Eur. Phys. J. E 37 (1) (2014).
- [16] P.R. Nayak, Random process model of rough surfaces, J. Lubr. Technol. 93 (398) (1971).
- [17] G. Carbone, B. Lorenz, B.N.J. Persson, A. Wohlers, Contact mechanics and rubber friction for randomly rough surfaces with anisotropic statistical properties, Eur. Phys. J. E 29 (275) (2009).
- [18] B.N.J. Persson, B. Lorenz, A.I. Volokitin, Heat transfer between elastic solids with randomly roughsurfaces, Eur. Phys. J. E 31 (3) (2010).
- [19] K.L. Johnson, Contact mechanics, Cambridge university press, 1987.
- [20] Private communication with brandon krick and gregory sawyer, 2021.
- [21] B.N.J. Persson, Theory of rubber friction and contact mechanics, J. Chem. Phys. 115 (3840) (2001).
- [22] B.N.J. Persson, Elastoplastic contact between randomly rough surfaces, Phys. Rev. Lett. 87 (116101) (2001).
- [23] B. Lorenz, B.N.J. Persson, On the dependence of the leak rate of seals on the skewness of the surface height probability distribution, EPL 90 (38002) (2010).
- [24] A. Tiwari, A. Almqvist, B.N.J. Persson, Plastic deformation of rough metallic surfaces, Tribol. Lett. 68 (1) (2020).

- [25] G.J.V. Amerongen, The permeability of different rubbers to gases and its relation to diffusivity and solubility, J. Appl. Phys. 17 (972) (1946).
- [26] C. Huon, A. Tiwari, C. Rotella, P. Mangiagalli, B. N. J. Persson, Air, Helium and Water Leakage in Rubber O-ring Seals with Application to Syringes, accepted in Tribol. Lett. https://doi.org/10.1007/s11249-022-01564-9.
- [27] B. Lorenz, B.N.J. Persson, Leak rate of seals: effective-medium theory and comparison with experiment, Eur. Phys. J. E 31 (159) (2010).
- [28] B. Lorenz, B.N.J. Persson, Leak rate of seals: comparison of theory with experiment, EPL 86 (44006) (2009).
- [29] W.B. Dapp, A. Lücke, B.N.J. Persson, M.H. Müser, Self-affine elastic contacts: percolation and leakage, Phys. Rev. Lett. 108 (244301) (2012).
- [30] W.B. Dapp, M.H. Müser, Fluid leakage near the percolation threshold, Sci. Rep., 6 (1) (2016) 1–8.
- [31] B.N.J. Persson, Interfacial fluid flow for systems with anisotropic roughness, Eur. Phys. J. E 43 (1) (2020).
- [32] A. Wang, M.H. Müser, Percolation and reynolds flow in elastic contacts of isotropic and anisotropic, randomly rough surfaces, Tribol. Lett. volume 69 (1) (2021).
- [33] B.N.J. Persson, Comments on the theory of fluid flow between solids with anisotropic roughness, Tribol. Lett. 69 (1) (2021).
- [34] M. Scaraggi, Lubrication of textured surfaces: a general theory for flow and shear stress factors, Phys. Rev. E 86 (026314) (2012).
- [35] M. Scaraggi, The friction of sliding wet textured surfaces: the bruggeman effective medium approach revisited, Proc. R. Soc. A: Math. Phys. Eng. Sci. 471 (20140739) (2015).

- [36] C. Yang, B.N.J. Persson, Contact mechanics: contact area and interfacial separation from small contact to full contact, J. Phys.: Condens. Matter 20 (215214) (2008).
- [37] L. Afferrante, F. Bottiglione, C. Putignano, B.N.J. Persson, G. Carbone, Elastic contact mechanics of randomly rough surfaces: an assessment of advanced asperity models and persson's theory, Tribol. Lett. 66 (1) (2018).
- [38] A. Almqvist, C. Campana, N. Prodanov, B.N.J. Persson, Interfacial separation between elastic solids with randomly rough surfaces: comparison between theory and numerical techniques, J. Mech. Phys. Solids 59 (2355) (2012).
- [39] A. Tiwari, B.N.J. Persson, Physics of suction cups, Soft Matter 15 (9482) (2019).
- [40] F.J. Fischer, K. Schmitz, A. Tiwari, B.N.J. Persson, Fluid leakage in metallic seals, Tribol. Lett. 68 (1) (2020).
- [41] A. Tiwari, A. Wang, M.H. Müser, B.N.J. Persson, Contact mechanics for solids with randomly rough surfaces and plasticity, Lubricants 7 (90) (2019).
- [42] N. Menga, Rough frictional contact of elastic thin layers: the effect of geometrical coupling, Int. J. Solids Struct. 164 (212) (2019).
- [43] N. Menga, G. Carbone, D. Dini, Exploring the effect of geometric coupling on friction and energy dissipation in rough contacts of elastic and viscoelastic coatings, J. Mech. Phys. Solids 148 (104273) (2021).
- [44] A. Almqvist, C. Campan, N. Prodanov, B.N.J. Persson, Interfacial separation between elastic solids with randomly rough surfaces: comparison between theory and numerical techniques, J. Mech. Phys. Solids 59 (2355) (2011).
- [45] B.N.J. Persson, C. Yang, Theory of the leak-rate of seals, J. Phys. Condensed Matter 20 (315011) (2008).